Progress in Reaction Kinetics and Mechanism

ARTICLE

Open Access

https://doi.org/10.48130/prkm-0025-0005

*Progress in Reaction Kinetics and Mechanism* **2025**, 50: e005

# A MEDT investigation of mechanism and selectivities of the intramolecular [3+2] cycloaddition reaction of (*E*)-*N*-((2-((methylbut-2-en-1-yl)thio)-1*H*-indol-3-yl)methylene)methanamine-oxide

Djamila Hellel[1,2], Fouad Chafaa[1,3], Hayet Bouabbaci[1] and Abdelmalek Khorief Nacereddine[1*]

[1] *Laboratory of Physical Chemistry and Biology of Materials, Department of Physics and Chemistry, Higher Normal School of Technological Education of Skikda, Azzaba 21300, Skikda, Algeria*

[2] *Laboratory of Applied Sciences and Didactics, Department of Physics and Chemistry , Higher Normal School of Laghouat, Laghouat, Algeria*

[3] *Department of Common Trunk, Faculty of Natural and Life Sciences University of Batna 2, Batna, Algeria*

* Corresponding author, E-mail: a.khorief@enset-skikda.dz

## Abstract

In this paper, an MEDT computational study was conducted through the B3LYP/6-31G(d,p) DFT method, to analyse the mechanism nature and the selectivities of the intramolecular [3+2] cycloaddition (I32CA) of the (*E*)-*N*-((2-((methylbut-2-en-1-yl)thio)-1*H*-indol-3-yl)methylene)methanamine oxide. The investigation covered the three potential pathways, including the fused *endo* and *exo* steric approaches and the bridged channels associated with the I32CA reaction. Analysis of relative energy indicated that the isoxazolidine formed from the *fused-endo* pathway is favored kinetically, which are consistent with the published experimental findings. Based on bond order values and geometry of the transition states, the obtained results suggest that this I32CA occurs via one-step slightly synchronous mechanism in the case of the *fused* modes, whereas in the bridged one via a one-step slightly asynchronous mechanism. Relative thermodynamic functions show that the studied I32CA has exothermic and exergonic behaviours. ELF analysis of the *fused-endo* pathway reveals that the mechanism of this I32CA reaction is non-concerted slightly synchronous two stages one-step. NCI and QTAIM analyses show that the existence of several NCIs at the favourable *fused-endo* structure is the main reason for the *fused-endo* selectivity.

**Citation:** Hellel D, Chafaa F, Bouabbaci H, Khorief Nacereddine A. 2025. A MEDT investigation of mechanism and selectivities of the intramolecular [3+2] cycloaddition reaction of (*E*)-*N*-((2-((methylbut-2-en-1-yl)thio)-1*H*-indol-3-yl)methylene)methanamine-oxide. *Progress in Reaction Kinetics and Mechanism* 50: e005 https://doi.org/10.48130/prkm-0025-0005

## Introduction

The broad range of beneficial biological activities exhibited by heterocyclic compounds and their derivatives makes them a crucial focus of pharmaceutical research. Several compounds used in medicine and pharmacy fields incorporate in their structure an heterocycle, in which extensive experimental and computational studies have been conducted to discover innovative and cost-effective methods to prepare these compounds[1]. The cycloaddition reactions, including the [3+2] cycloaddition reaction[2], represent a key method to synthesising a variety of heterocycles[3,4]. The 32CA reaction is a highly significant process for constructing heterocyclic five-membered rings. It offers a straightforward approach to preparing these important structures having several chiral centers, providing good control of stereoselectivity[5]. Today, the main challenge in organic chemistry is the control of stereoselectivity during the reaction. Among the developed methods[6], the most important are ones that employ the reagents and change the reaction conditions leading to obtaining different isomers. Other reagents[7], temperature[8], and solvent[9] were utilized to reverse the enantioselectivity, and thus both enantiomers could be prepared. Scientists have become interested in synthesizing heterocycles with enhanced biological activities due to the broad range of applications of these compounds. Heterocycles serve as vital frameworks in the modulation of drug polarity by replacing functional groups, thereby increasing bioavailability[10].

The structure of indole is a significant nucleus found in synthetic or natural compounds with important biological properties[11]. The thiopyranoindole heterocycles are also noteworthy due to their medicinal properties[12]. Among the important heterocycles, the isoxazolidines have a particular importance and are considered a useful class abundant in compounds[13]. Some isoxazolidine derivatives exhibit antifungal[14], anti-inflammatory[15], antimycobacterial[16], and cytotoxic activities[17], and they also act as DNA intercalators[18].

The C-S bond has shown promising potential as a target for the development of new drugs. Several studies have shown that compounds containing a C-S bond can exhibit interesting anticancer, antifungal, and antimicrobial properties[19]. In addition, current drugs such as sulfonamides and thiazolidinones contain C-S bonds and are used to treat several diseases, namely, diabetes, cardiovascular diseases, and bacterial infections. These examples suggest that the C-S bond may be an important fragment for the discovery of new biologically active molecules[20].

Over the past few years, there has been significant experimental and theoretical research carried out on intramolecular 32CA reactions that have been performed to investigate and discover the factors controlling the selectivity in this category of CA reactions[21–26].

The question of stereoselectivity is a consequence of the balance between steric and electronic effects. Thus, controlling the stereoselectivity at the cyclisation step is a great challenge in the organic synthesis field. This can be achieved by selecting appropriate reactants or by employing a molecular complex as a catalyst[27], especially in the case when cycloaddition reactions occur through a stepwise mechanism[28–30]. Molecular electron density theory (MEDT)[31] investigations revealed a connection between the reactivity of 32CA reactions, which involve the most basic three-atom components

(TACs), and their electronic structure. This methodology has successfully provided a relation between the reactivity of the separated molecules and their electronic structure[32].

Nitrones are three-atom-components (TACs)[33] having a *zwitterionic*-type (*zw-type*) structure[32]. The intramolecular [3+2] cycloaddition (I32CA) reactions between TACs and alkenes involve heterocyclic structures through either bridged or fused modes. This method is highly versatile and efficient in creating complex heterocyclic architectures, which consist of oxygen and nitrogen atoms in a ring with five atoms (Fig. 1).

Furthermore, these modes allow for the construction of stereo- and regio-selective compounds. The resulting heterocyclic architectures are highly valuable in many applications, namely, pharmaceutical chemistry, where, the specific arrangement of atoms can greatly impact the compound's properties and potential applications. Overall, the I32CA reactions of nitrones provide a valuable tool for synthesizing complex, highly specific heterocyclic structures with diverse applications[34,35].

Majumder & Bhuyan[36] described the preparation of new dihydroisoxazole/tetrahydroisoxazole annulated thiopyrano[2,3-b]indole obtained from oxindole through I32CA reaction (Fig. 2). This synthetic method has allowed for the production of innovative compounds that may have potential applications in the fields of medicinal or pharmaceutical chemistry.

Herein, we aimed to conduct a computational analysis with the goal of analysing the selectivity observed in the experimental results reported by Majumder & Bhuyan[36], as well as to understand in a deep manner the factors governing the selectivity and to elucidate their influence on the mechanism of this I32CA reaction.

## Methods employed for computational analysis

Previous DFT investigations indicate that the use of the B3LYP/6-31G(d,p) method explained correctly the experimental observations of cycloaddition reactions[37–39]. Thereby, in this work, all calculations were performed within the B3LYP/6-31G(d,p) computational level[40]. The frequency calculations of the optimized geometry of stationery points, namely, reactants, transition states (TSs), and cycloadducts (CAs) were characterized to ensure that only TSs possessed a single imaginary frequency (for more details, refer to the ESI). Thermodynamic functions were computed in toluene at 383.15 K and 1 atm, based on the optimized structures in the gas phase[41], then scaled by a factor of 0.96[42]. The atomic charges of TS structures were computed within the natural bond orbital (NBO) method[43]. For the study of toluene solvation effects, single-point calculations were performed through the optimized gas phase structures using self-consistent reaction fields (SCRF)[44] within the polarisable continuum model (PCM)[45]. These calculations have been realized using the Gaussian 09 package[46].

The electron localization function (ELF)[47] analysis has been conducted using Multiwfn software[48]. The non-covalent interaction (NCI) study has been realized through the analysis of the reduced density gradient together with the low-gradient isosurfaces[49], which was obtained from the NCI plot[50]. QTAIM analysis[51] were conducted using Multiwfn software[48].

## Results and discussion

### Energy and geometry analysis

Previous theoretical studies have shown that the majority of 32CA reactions occur via a mechanism of one step[52–54]. Therefore, in this study, we have exclusively focused on this mechanism for the I32CA reaction of (*E*)-*N*-((2-((-methylbut-2-en-1-yl)thio)-1*H*-indol-3-yl)-methylene)methanamine oxide **1**. Thereby, we have identified and characterized three TSs and their corresponding CAs, in relation to the potential regio- and stereo-selective approaches. Therefore, the present I32CA reaction can proceed through two regioisomeric channels, the *fused* or *bridged* one (Fig. 3).

The Cartesian coordinates of **1**, TSs, and CAs are shown in Supplementary Table S1 together with the values of imaginary

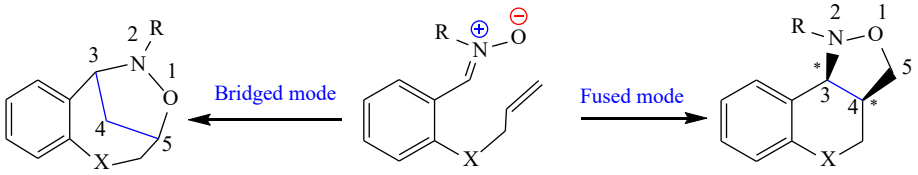


**Fig. 1** The possible reactive channels of the I32CA reaction.

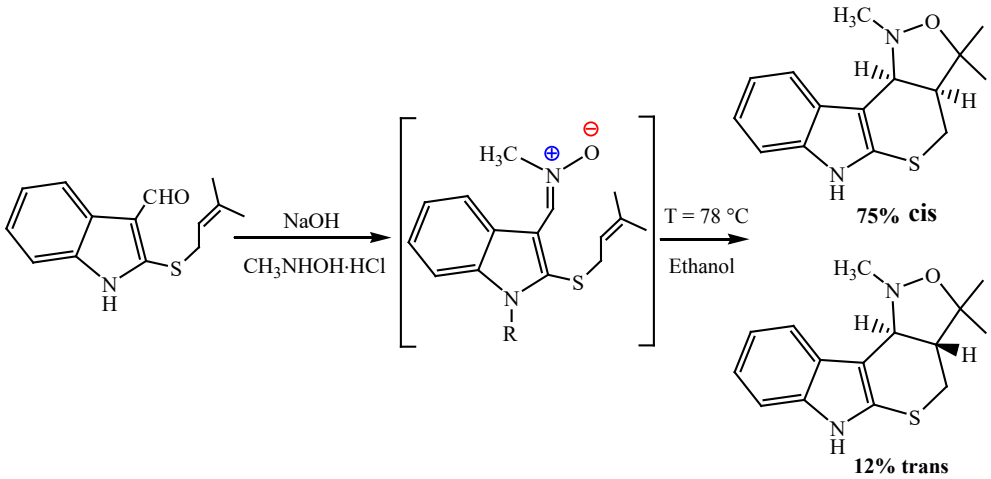


**Fig. 2** The synthesis of tetracyclic isoxazolidines from a simple oxindole.

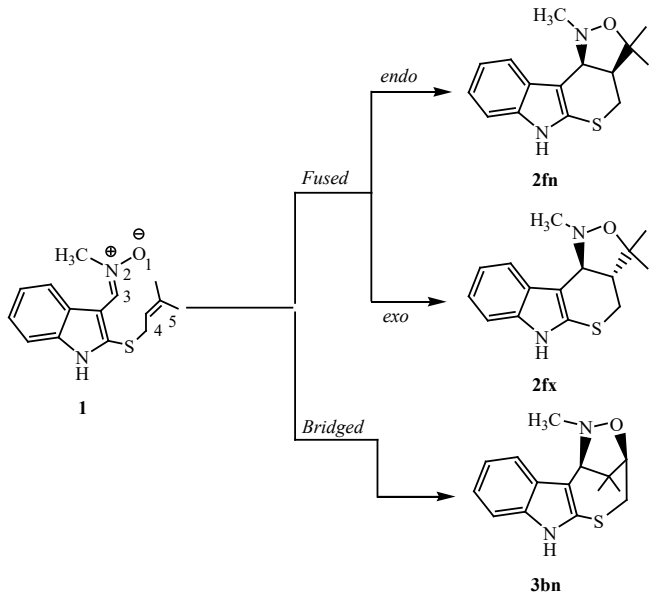


**Fig. 3** Reactive pathways associated with the I32CA of 1.

frequencies of TSs. Values of relative energies corresponding to (*E*)-*N*-((2-((-methylbut-2-en-1-yl)thio)-1*H*-indol-3-yl)methylene)methanamine oxide **1**, and TSs and CAs are shown in Table 1, whereas absolute energy values are given in Supplementary Table S2. The energetic profiles in the toluene solvent of the three corresponding pathways are given in Fig. 4.

According to the values in Table 1, we notice from an analysis between the ΔE values in gas-phase for the possible reactive routes in the studied I32CA reaction that the *fused-endo* mode (Ea = 18.8 kcal/mol) is the kinetically favoured cycloadduct. The relative energy difference (ΔΔE) of 11.8 kcal/mol between $E_a$ of *fused-endo* and the second most favorable pathway, the *bridged-endo* pathway. Additionally, it is observed that all reactive routes are irreversible because the corresponding cycloadducts are more stable than reactant **1** ($\Delta E_{cycloaaducts} < 0$). Moreover, the *bridged* cycloadduct is less stable compared with the *fused* ones, which may be attributed to the ring strain presented in the *bridged* ring. Thus, the bridged ring that is characterized by a seven-membered ring that is unstable than one having six atoms formed from the *fused* channel. Note that the obtained large activation energies also suggest that these I32CA reaction pathways proceed via a low-polar mechanism[55,56].

On the other hand, we notice that the cycloadduct favoured kinetically is stable, confirming that the studied I32CA is under kinetic control. These findings are in perfect accordance with the data observed experimentally. The optimised structures of TSs associated with the I32CA of (*E*)-*N*-((2-((methylbut-2-en-1-yl)thio)-1*H*-indol-3-yl)methylene)methanamine oxide **1** are depicted in Fig. 5, as well as the distances and the Wiberg bond order (BO) of the bonds under formation.

In the fused structures, the distances of the O–C and C–C bonds are respectively 1.97 and 2.23 Å at **TS2n**, and 2.05 and 2.18 Å at **TS2x**. In contrast, in the bridged structure (**TS3n**), these bond lengths are 2.07 and 2.12 Å. Also, the distance of the C–C bond is larger than that of the O–C bond in all three TS structures, suggesting a synchronicity mechanism in both modes.

Using Wiberg bond indices[57], the BO analysis for the two regioisomeric pathways indicates that the C–C bond formation is generally advanced slightly compared to that of the O–C, with the exception of the favorable transition state, **TS2n**, we notice the opposite, in which the formation of O–C bonds is slightly advanced

**Table 1.** Values of relative energies of (*E*)-*N*-((2-((-methylbut-2-en-1-yl)thio)-1*H*-indol-3-yl)methylene)methanamine oxide 1, TSs, and CAs in gas-phase and solution of toluene.

| System | $\Delta E_{Gas\ phase}$ (kcal/mol) | $\Delta E_{Toluene}$ (kcal/mol) |
|---|---|---|
| **TS2n** | 18.7 | 21.8 |
| **TS2x** | 34.9 | 37.0 |
| **TS3n** | 30.5 | 31.8 |
| **CA2n** | −17.5 | −15.3 |
| **CA2x** | −13.3 | −12.1 |
| **CA3n** | −9.1 | −7.7 |

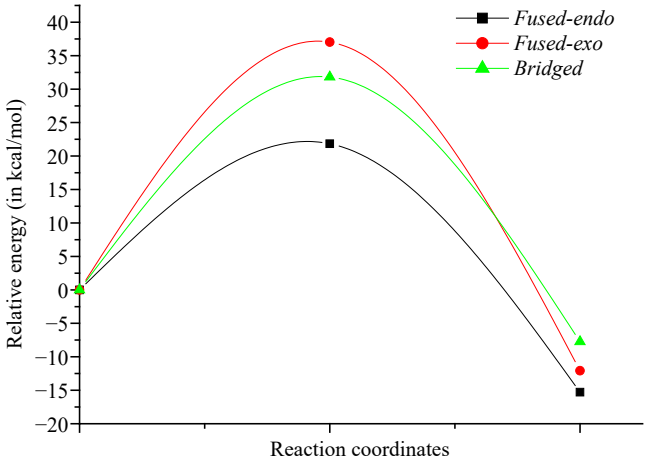


**Fig. 4** Curves of energy profiles in toluene solvent of the I32CA reactive paths of (*E*)-*N*-((2-((methylbut-2-en-1-yl)thio)-1*H*-indol-3-yl)methylene)methanamine oxide 1.

compared with the other C–C. This highlights a slight asynchronous bonding process. These BO values support a previously predicted asynchronous mechanism.

Since this I32CA reaction of (*E*)-*N*-((2-((methylbut-2-en-1-yl)thio)-1*H*-indol-3-yl)methylene)methanamine oxide **1** was conducted in toluene and because of solvation effects that may influence on the energy values, a supplementary single-point calculation taking into account the toluene solvent through the gas-phase optimized structures were performed (see Table 1). Also, we noticed that by inclusion of toluene solvent effects in the calculations, the reactant, TSs, and CAs become more stable in comparison with gas-phase results. Including solvent effects led to increases in activation energies by 3.1, 2.1, and 1.3 kcal/mol for **TS2n**, **TS2x**, and **TS3n** respectively. In addition, the solvation effects also reduced slightly the reaction's exothermicity by 2.2, 1.2, and 1.4 kcal/mol for **CA2n**, **CA2x**, and **CA3n** respectively. These results may be explained by the improvement of solvation of (*E*)-*N*-((2-((methylbut-2-en-1-yl)thio)-1*H*-indol-3-yl)methylene)methanamine oxide **1** relative to the TSs and CAs in polar solvents[58]. Despite these changes, the regioselectivity and stereoselectivity patterns observed in the gas phase stay the same.

Table 2 provides the values of thermodynamic functions for the I32CA reaction of (*E*)-*N*-((2-((methylbut-2-en-1-yl)thio)-1*H*-indol-3-yl)methylene)methanamine oxide **1**, while absolute values are shown in Supplementary Table S3.

From the values of the activation enthalpies corresponding to the three competing reactive paths, we remark that the *fused-endo* path (**TS2n**) has the lowest value (20.7 kcal/mol), which is considered the most favourable reactive pathway, leading to the construction of the tetracyclic isoxazolidine **CA2n**. In addition all reactive pathways are characterised by a negative sign of relative enthalpy associated

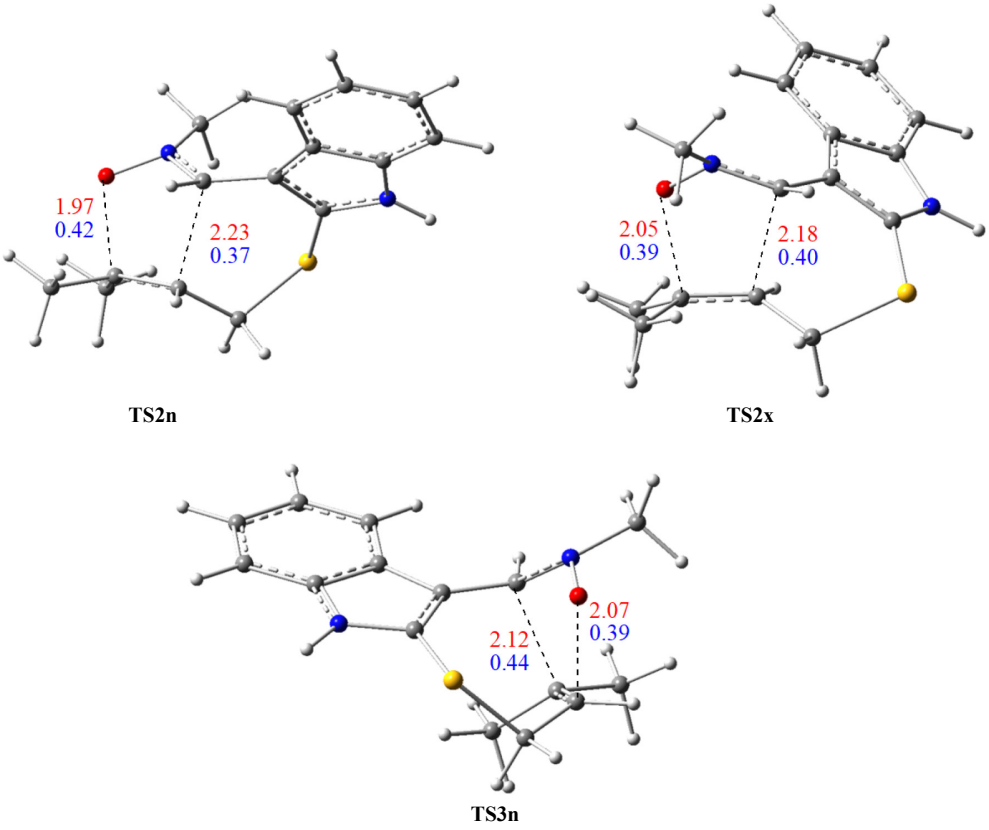


**Fig. 5** TSs optimised structures of the I32CA of (*E*)-*N*-((2-((methylbut-2-en-1-yl)thio)-1*H*-indol-3-yl)methylene)methanamine oxide 1, showing the lengths (in Å, in red), and BO (in blue) of bonds under formation.

**Table 2.** Relative thermodynamic function values for the TSs and CAs of the I32CA of (*E*)-*N*-((2-((methylbut-2-en-1-yl)thio)-1*H*-indol-3-yl)methylene)methanamine oxide **1**.

| System | ΔH (kcal/mol) | ΔS (cal/mol/K) | ΔG (kcal/mol) |
|---|---|---|---|
| **TS2n** | 20.8 | −22.2 | 28.6 |
| **TS2x** | 35.7 | −20.3 | 42.8 |
| **TS3n** | 30.8 | −23.3 | 38.9 |
| **CA2n** | −14.5 | −26.6 | −5.2 |
| **CA2x** | −11.3 | −24.8 | −2.6 |
| **CA3n** | −7.1 | −27.4 | 2.5 |

to the cycloadducts, which account for an exothermic character for this I32CA reaction.

Given the intramolecular nature of the studied reaction, these pathways exhibit low entropy values. Adding entropic contributions increases the value of relative Gibbs free energy to reach 28.6 kcal.mol$^{-1}$ for the most favoured cycloadduct **CA2n**. The activation enthalpies for **TS2x** and **TS3n** are 35.7 and 30.8 kcal/mol, respectively, in which their free activation energies reaching respectively, 42.8 and 38.9 kcal/mol. Therefore, the *fused-exo* and *bridged* modes are less favorable pathways in this I32CA reaction that produce exclusively the **CA2n**, in great agreement with what observed experimentally[36]. Likewise, the relative free energy of the cycloadducts show that the pathways associated with fused mode are exergonic character but that of the bridged one is endergonic.

## Analysis of the natural molecular mechanism

To study the molecular mechanism type of the present I32CA, we opted for the ELF topological analysis[47]. Thereby, after deep analysis of the IRC curve of the favorable *fused-endo* channel, we have selected some pertinent channels for this analysis. The curve IRC of the favourable **TS2n** as well as the selected point positions, **MC2n**, **TS2n**, **P$_1$**, **P$_2$**, **P$_3$**, **P$_4$**, **P$_5$**, and **CA2n** associated with this pathway are illustrated in Supplementary Fig. S1. The electron density of the pertinent electronic basins obtained from ELF analysis on the structure corresponding to studied points on the IRC curve are collected in Table 3. Figure 6 shows the structure of different selected points together with the position of the ELF valence basins attractor.

**Table 3.** Electron density of the pertinent basins of the chosen points on the reactive *fused-endo* pathways of the I32CA of **1**.

| | **MC2n** | **TS2n** | **P$_1$** | **P$_2$** | **P$_3$** | **P$_4$** | **P$_5$** | **CA2n** |
|---|---|---|---|---|---|---|---|---|
| d(C3–C4) | 2.91 | 1.97 | 1.77 | 1.66 | 1.57 | 1.54 | 1.48 | 1.47 |
| d(O1–C5) | 3.01 | 2.23 | 2.00 | 1.87 | 1.75 | 1.71 | 1.62 | 1.58 |
| V(O1–N2) | 1.31 | 1.10 | 1.00 | 0.95 | 0.91 | 0.88 | 0.88 | 0.86 |
| V(N2–C3) | 3.98 | 2.49 | 2.13 | 1.95 | 1.88 | 1.84 | 1.83 | 1.83 |
| V(C4–C5) | 1.81, 1.75 | 2.86 | 2.28 | 2.13 | 2.06 | 2.01 | 2.00 | 1.99 |
| V(C3…C4) | – | – | – | 1.64 | 1.74 | 1.81 | 1.84 | 1.86 |
| V(O1…C5) | – | – | 0.30 | 0.78 | 0.98 | 1.09 | 1.15 | 1.16 |
| V(C3) | – | 0.43 | 0.63 | – | – | – | – | – |
| V(C4) | – | 0.55 | 0.82 | – | – | – | – | – |
| V(O1) | – | – | – | – | – | – | – | – |
| V(C5) | – | – | – | – | – | – | – | – |

The most important basins in this molecular system corresponding to the reactive regions of **1**, are the (C3–N2 and N2–O1), and C4–C5 (for atom numbering see Fig. 3).

The structure of **MC2n** is characterized by V(N2,C3) disynaptic basin with 3.98 e of population, accounting for the double-bond character of this region. Also, the O1–N2 shows disynaptic basin V(O1,N2) which integrating of 1.31 e. Moreover, the reactive region C4–C5 has two disynaptic basins, V(C4,C5) and V'(C4,C5)

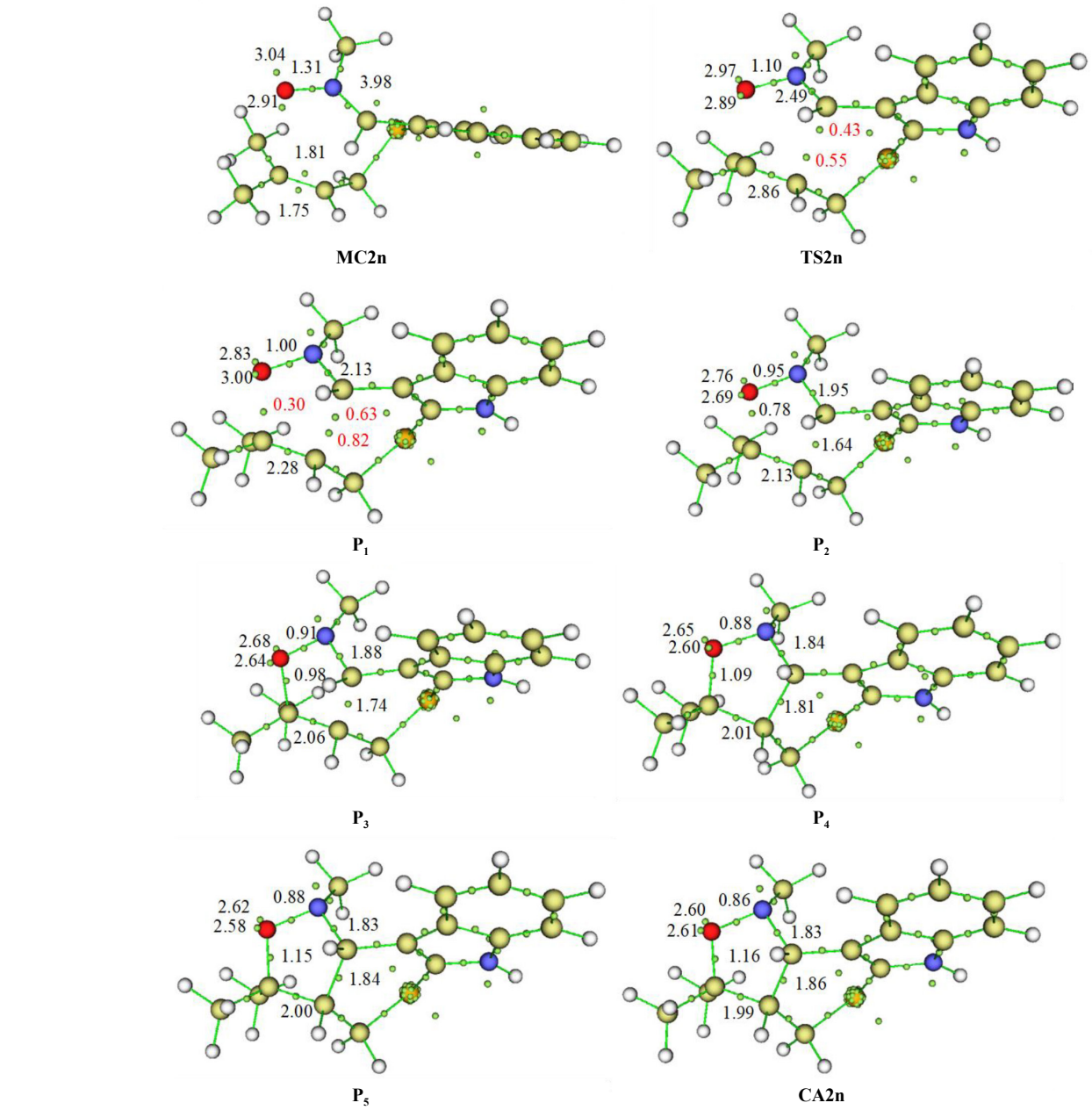


**Fig. 6** Structure of different selected points together with the position of the ELF valence basin attractors of the chosen structures corresponding to the *fused-endo* pathways of the I32CA of **1**.

characterised by a total electronic population equal to 3.56 e, indicating a double bond character of this reactive region.

At the second point **TS2n**, in which d(C3…C4) = 2.23 Å and d(O1…C5) = 1.97 Å, the population of the C3–N2 region that is has a disynaptic basin V(C3–N2) decreased to becomes 2.49 e, leading to the appearance of one new monosynaptic basin V(C3), with a 0.43 e. Another new monosynaptic basin V(C4) with 0.55 e appeared at this point produced from the disappearance of V'(C4,C5) disynaptic basin at this point, which leads to C4–C5 only having a monosynaptic basin integrating 2.86 e.

At $\mathbf{P_1}$, where the distances of the C3…C4 and O1…C5 are respectively 2.00 and 1.77 Å, we remark an apparition of new disynaptic basin V(O1,C5) integrate 0.30 e. In addition to this change, we notice an increase of the electronic population of V(C3) and V(C4) monosynaptic basins to become, 0.63 and 0.82 e respectively, generating from the depopulation of the disynaptic basins V(C4,C5) and V(C3,N2) which become 2.28 and 2.13 e respectively.

At $\mathbf{P_2}$, characterised by d(C3…C4) = 1.87Å and d(O1…C5) = 1.66 Å, the important evolution is the generation of a new V(C3,C4) disynaptic basin characterized by 1.64 e, accounting that the second new C3–C4 single bond is formed. Also, we notice an increase in the electron density of V(O1,C5) disynaptic basin which becomes 0.78 e.

At $\mathbf{P_3}$, in which d(O1–C5) = 1.57Å and d(C3–C4) = 1.75Å, the remarkable changes are the augmentation in the population of the new disynaptic basins V(C3,C4) and V(O1 C5) by slight values of 0.10 and 0.20 e to reach respectively 1.74, and 0.98 e. This increase in electron density of the newly forming disynaptic basins is accompanied by a decrease of that associated to the V(C4,C5) and V(N2,C3) which become 2.06 and 1.88e respectively.

At $\mathbf{P_4}$, in which d(O1–C5) = 1.54 Å and d(C3–C4) = 1.71 Å, the main development in electronic mechanism is only a slight increase in the population of the disynaptic basins V(O1,C5) and V(C3,C4) to become 1.09 and 1.81 e respectively.

At **$P_5$**, in which d(O1–C5) = 1.47 Å and d(C3–C4) = 1.62 Å, there is no noticeable topological change except the slight augmentation in the population of disynaptic basins V(C3,C4) and V(O1,C5) by 0.03 and 0.06 e, to become 1.84 and 1.15 e, respectively.

At the cycloadduct **CA2n**, where d(O1–C5) = 1.47 Å and d(C3–C4) = 1.62 Å, the population associated with disynaptic basins V(O1,C5) and V(C3,C4) continue to increase by 0.01 and 0.02 e to reach 1.86 and 1.16 e respectively.

From this analysis, we can conclude that the mechanism of this I32CA reaction is *two-stage one-step*[59] , where, the O1–C5 single bond formation begins first, followed by that of the second C3–C4.

## Origin of the *fused-endo* stereoselectivity

### *NCI analysis*

Based on our prior computational studies showing that NCIs are the main cause for the stereoselectivity observed in the 32CA reactions[60–63] thereby, a supplementary analysis of the structure associated to **TS2n** and **TS2x** is necessary to discover the main reason of the *fused-endo* selectivity. Figure 7 illustrates the NCI density gradient isosurfaces for **TS2n** and **TS2x**.

From Fig. 7 we observe the existence of green surface in the zone located between the carbon atom of the alkene fragment and the oxygen of nitrone framework **1** in both **TS2n** and **TS2x** that may be due to the interactions of the newly forming O1…C5 and C3…C4 bonds. On the other hand, we observe the existence of several green surfaces in **TS2n** structure that are considered as indices for the existence of weak NCIs. Otherwise, we note that **TS2x** is characterized by a small green surface and large red surface that are associated with steric hindrances that decrease the stability of this structure.

To confirm the existence of NCIs at these structures, we have realized a supplementary analysis based on the reduced density gradient, in which Fig. 8 shows the low-gradient isosurfaces for **TS2n** and **TS2x**. The low-gradient isosurfaces associated with **TS2n** show the existence of four low-density gradient spikes at −0.005, −0.008, −0012, and −0.020 a.u, account for the formation of four favourable NCIs. On the other hand, the low-gradient isosurfaces corresponding to **TS2x** shows the existence of only two low-density gradient spikes at −0.005 and −0.010 a.u. The presence of several favorable NCIs in **TS2n** is the main reason of its stability in comparison with **TS2x** that have only two NCIs.

### *QTAIM study*

QTAIM study of the electron density $\rho$ produces some critical points (cps), that are points on the molecular system characterized by $\nabla\rho(\mathbf{r}) = 0$[51]. The existence of (3,−1) cp gives the link between basins of atoms adjacent, named as bond critical point (bcp). Previous studies show that the force of such interaction, especially hydrogen bond (HB) may be evaluated using the properties of its bcp[64,65]. Rozas et al.[64] proposed that these interactions may be distinguished into three types; the strong interaction have a negative Laplacian ($\nabla^2\rho_{bcp} < 0$) and a negative total electron energy density ($H_{bcp} < 0$). For, the second type that is a medium strength interaction, which defined by ($\nabla^2\rho_{bcp} < 0$) and ($H_{bcp} > 0$). The last type is weak interaction are characterized by ($\nabla^2\rho_{bcp} > 0$) and ($H_{bcp} > 0$).

For distinguishing between the NCS presented at both **TS2n** and **TS2x**, a QTAIM study[51] at these structures have been realized, in which the values of total electron density, total electron energy density and Laplacian of the (3,−1) cps are given in Table 4. Figure 9 illustrates the schematisation of the QTAIM molecular graphs associated to **TS2n** and **TS2x** that are obtained from the QTAIM study.

Figure 9 shows that except the interactions associated with the forming bonds, **TS2n** has two NCIs that are H…H and H…S, while

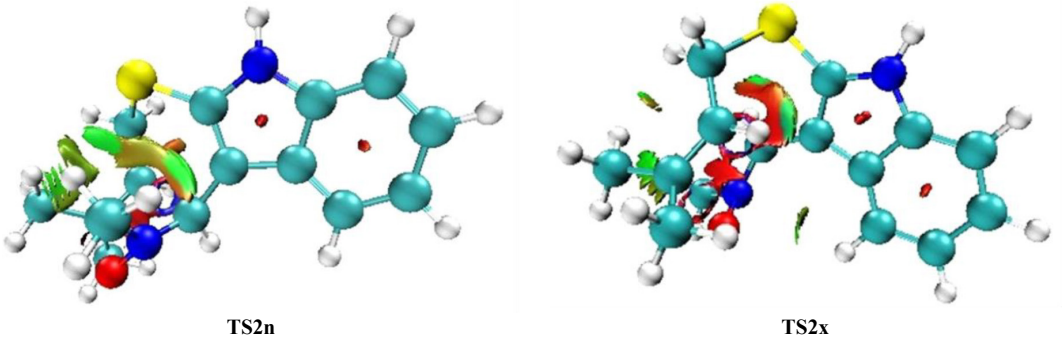


**Fig. 7** NCI analysis of **TS2n** and **TS2x** structures with isosurfaces = 0.40.

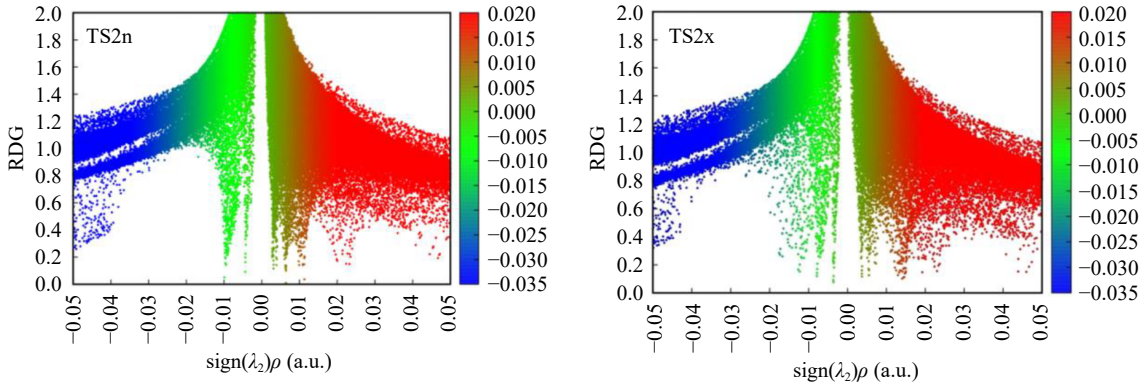


**Fig. 8** Plots of RDG for **TS2n** and **TS2x** structures.

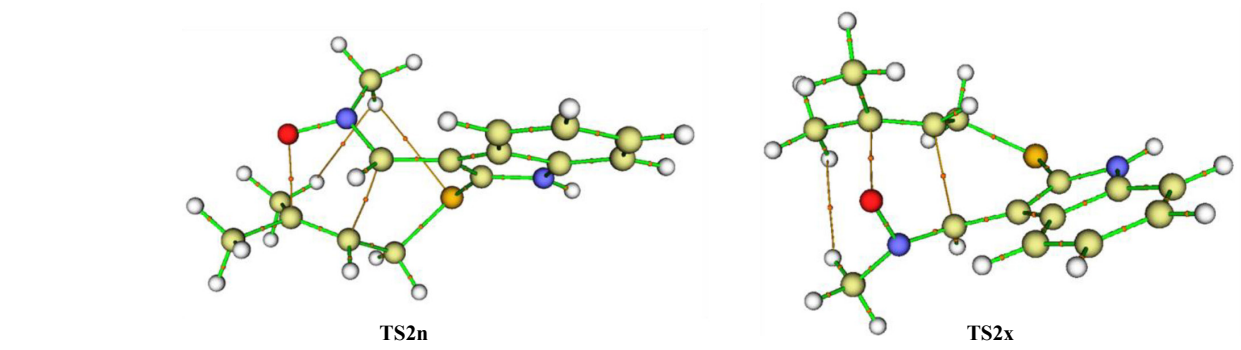


**Fig. 9** QTAIM molecular schematisation of TS2n and TS2x together with bond paths and (3,–1) critical points.

**Table 4.** QTAIM parameters associated with the (3,–1) cps associated with **TS2n** and **TS2x**.

| | Interaction | $\rho_{cbcp}$ | $\nabla^2\rho_{bcp}$ | $H_{bcp}$ |
|---|---|---|---|---|
| **TS2n** | O1…C5 | 0.79 | 0.12 | -0.15 |
| | C3…C4 | 0.58 | 0.43 | 0.13 |
| | H…H | 0.44 | 0.16 | 0.99 |
| | H…S | 0.99 | 0.32 | 0.15 |
| **TS2x** | O1…C5 | 0.69 | 0.18 | -0.97 |
| | C3…C4 | 0.65 | 0.33 | -0.16 |
| | H…H | 0.30 | 0.81 | 0.30 |

**TS2x** has only one H…H NCI type. Thereby, the stabilisation of **TS2n** may be attributed to the presence of a supplementary H…S NCI.

Table 4 shows that all (3,-1) bcps associated with H…H and H…S interactions presented both in **TS2n** and **TS2x** are characterized by $\nabla^2\rho_{bcp} > 0$ and $H_{bcp} > 0$. Thereby, they may be classified as weak strength interactions according to the classification of Rozas et al.[64]. On the other hand, we remark that only O1…C5 in both structures and C3…C5 in **TS2x** have negative total electron energy density ($H_{bcp} < 0$) because they are attributed to the forming bonds, which are considered as strong interactions.

## Conclusions

In this study, we conducted a theoretical analysis of the molecular mechanism, regioselectivity, and stereoselectivity of the I32CA reaction of (*E*)-*N*-((2-((methylbut-2-en-1-yl)thio)-1*H*-indol-3-yl)methylene)methanamine oxide **1**, derived from 2-((2-methylprop-1-en-1-yl)thio)-1*H*-indole-3-carbaldehyde through MEDT within the B3LYP/6-31G(d,p) DFT method. Our main findings are as follows:

(i) The B3LYP/6-31G(d,p) computational level, accurately explains the regio- and stereo-selectivity observed experimentally.

(ii) The I32CA reaction occurs under kinetic control leading to formation of a single cycloadduct obtained from compound **1**.

(iii) Analysis of the TSs as well as bond order indices indicates that this I32CA reaction occurs through a *one-step* slightly asynchronous mechanism.

(iv) The effect of solvation increases the activation energies but does not modify the gas phase selectivity patterns.

(v) The studied I32CA is characterized by exothermic behaviour for all reactive pathways and exergonic behaviour for the fused paths and an endergonic for the bridged one.

(vi) Bond distance analysis of the forming bond at the TSs shows that this I32CA reaction precedes through a slightly asynchronous mechanism.

(vii) ELF study shows that this I32CA occurs through a non-concerted *two stage one-step* mechanism.

(viii) NCI and QTAIM topological analyses indicate that the stabilisation of the favoured **TS2n** is attributed to the presence of several weak NCIs.

## Author contributions

The authors confirm contribution to the paper as follows: study conception and design: Hellel D, Bouabbaci H, Chafaa F; data collection: Hellel D, Chafaa F, Khorief Nacereddine A; analysis and interpretation of results: Hellel D, Chafaa F, Bouabbaci H, Khorief Nacereddine A; draft manuscript preparation: Hellel D, Chafaa F, Khorief Nacereddine A. All authors reviewed the results and approved the final version of the manuscript.

## Data availability

All data generated or analyzed during this study are included in the published article and its supplementary information files.

## Acknowledgments

This study was carried out within the framework of the PRFU project Code: B00L01EN210120220001 of the Ministry of Higher Education and Scientific Research of the Algerian Government.

## Conflict of interest

The authors declare that they have no conflict of interest.

**Supplementary information** accompanies this paper at (https://www.maxapress.com/article/doi/10.48130/prkm-0025-0005)

## Dates

Received 2 January 2025; Revised 5 February 2025; Accepted 17 February 2025; Published online 26 March 2025

## References

1. Pizzuti L, Mrcia SF, Alex FC, Frank H, Claudio MP. 2012. Recent advances in the ultrasound-assisted synthesis of azoles. In *Green Chemistry - Environmentally Benign Approaches*, eds. Mishra NK, Kidwai M. Rijeka: InTech. doi: 10.5772/35171
2. Carruthers W (ed.). 1990. 1,3-dipolar cycloaddition reactions. In *Tetrahedron Organic Chemistry Series*. Vol. 8. UK: Pergamon Press. pp. 269–331. doi: 10.1016/B978-0-08-034712-7.50011-4
3. Dake G. 2002. Cycloaddition reactions in organic synthesis. *Synthesis* 2002(10):1467
4. Kras J, Sadowski M, Zawadzińska K, Nagatsky R, Woliński P, et al. 2023. Thermal [3+2] cycloaddition reactions as most universal way for the

effective preparation of five-membered nitrogen containing heterocycles. *Scientiae Radices* 2:247–67
5. Padwa A, Pearson WH. 2003. *Synthetic applications of 1,3-dipolar cycloaddition chemistry toward heterocycles and natural products*. Volume 59. New York: John Wiley & Sons. doi: 10.1002/0471221902
6. Sibi M, Liu M. 2001. Reversal of stereochemistry in enantioselective transformations. Can they be planned or are they just accidental? *Current Organic Chemistry* 5:719–55
7. Gothelf KV, Hazell RG, Joergensen KA. 1998. ChemInform abstract: molecular sieve dependent absolute stereoselectivity in asymmetric catalytic 1, 3-dipolar cycloaddition reactions. *ChemInform* 29:51150
8. Otera J, Sakamoto K, Tsukamoto T, Orita A. 1998. Temperature-effected tuning of enantioselectivity in asymmetric catalysis. *Tetrahedron Letters* 39:3201–4
9. Zhou J, Ye MC, Huang ZZ, Tang Y. 2004. Controllable enantioselective Friedel-Crafts reaction between indoles and alkylidene malonates catalyzed by pseudo-*C3*-symmetric trisoxazoline copperII complexes. *Journal of Organic Chemistry* 69:1309–20
10. Gomtsyan A. 2012. Heterocycles in drugs and drug discovery. *Chemistry of Heterocyclic Compounds* 48:7–10
11. Ishikura M, Abe T, Choshi T, Hibino S. 2013. Simple indole alkaloids and those with a non-rearranged monoterpenoid unit. *Natural Product Reports* 30:694–752
12. Kumar S, Pany SPP, Sudhakar S, Singh SB, Todankar CS, et al. 2022. Targeting parallel topology of G-quadruplex structures by indole- fused quindoline scaffolds. *Biochemistry* 61:2546–59
13. Zawadzińska-Wrochniak K, Zavecz I, Hirka S. 2024. The recent progress in the field of the applications of isoxazoles and their hydrogenated analogs: mini review. *Scientiae Radices* 3:228–47
14. Leelananda SP, Lindert S. 2016. Computational methods in drug discovery. *Beilstein Journal of Organic Chemistry* 12:2694–718
15. Green MJ, Tiberi RL, Friary R, Lutsky BN, Berkenkoph J, et al. 1982. Synthesis and topical antiinflammatory activity of some steroidal [16$\alpha$,17$\alpha$-d] Isoxazolidines. *Journal of Medicinal Chemistry* 25:1492–95
16. Raunak, Kumar V, Mukherjee S, Poonam, Prasad AK, et al. 2005. Microwave mediated synthesis of spiro-(indoline-isoxazolidines): mechanistic study and biological activity evaluation. *Tetrahedron* 61:5687–97
17. Wu Y, Dai GF, Yang JH, Zhang YX, Zhu Y, et al. 2009. Stereoselective synthesis of 15- and 16-substituted isosteviol derivatives and their cytotoxic activities. *Bioorganic & Medicinal Chemistry Letters* 19:1818–21
18. Rescifina A, Chiacchio MA, Corsaro A, De Clercq E, Iannazzo D, et al. 2006. Synthesis and biological activity of isoxazolidinyl polycyclic aromatic hydrocarbons: potential DNA intercalators. *Journal of Medicinal Chemistry* 49:709–15
19. Zeyrek CT, Koçak SB, Hüseyin Ü, Pektaş S, Başterzi NS, et al. 2015. Molecular structure and density functional modelling studies of 2-[(E)-2-(4-hydroxyphenyl)ethyliminomethyl] phenol. *Journal of Molecular Structure* 1100:570–81
20. Balogun TA, Chukwudozie OS, Ogbodo UC, Junaid IO, Sunday OA, et al. 2022. Discovery of putative inhibitors against main drivers of SARS-CoV-2 infection: Insight from quantum mechanical evaluation and molecular modeling. *Frontiers in Chemistry* 10:964446
21. Sennikova VV, Zalaltdinova AV, Sadykova YM, Khamatgalimov AR, Gazizov AS, et al. 2022. Diastereoselective synthesis of novel spiro-phosphacoumarins and evaluation of their anti-cancer activity. *International Journal of Molecular Sciences* 23:14348
22. Duret G, Quinlan R, Yin B, Martin RE, Bisseret P, et al. 2017. Intramolecular inverse electron-demand [4+2] cycloadditions of ynamides with pyrimidines: scope and density functional theory insights. *Journal of Organic Chemistry* 82:1726–42
23. Chafaa F, Nacereddine AK, Djerourou A. 2020. A combined topological ELF, NCI and QTAIM study of mechanism and hydrogen bond controlling the selectivity of the IMDC reaction of nitrone-alkene obtained from m-allyloxybenzaldehyde. *Letters in Organic Chemistry* 17:260–67
24. Domingo PLR, Ríos-Gutiérrez DM, Adjieufack AI, Ndassa PIM, Nouhou CN, et al. 2018. Molecular electron density theory study of fused regioselectivity in the intramolecular [3+2] cycloaddition reaction of cyclic nitrones. *ChemistrySelect* 3:5412–20
25. Jasiński R. 2023. On the question of selective protocol for the preparation of juglone *via* (4+2) cycloaddition involving 3-hydroxypyridazine: DFT mechanistic study. *Chemistry of Heterocyclic Compounds* 59:179–82
26. Jasiński R. 2013. Competition between the one-step and two-step, zwitterionic mechanisms in the [2+3] cycloaddition of gem-dinitroethene with (*Z*)-*C*,*N*-diphenylnitrone: a DFT computational study. *Tetrahedron* 69:927–32
27. Gothelf AS, Gothelf KV, Hazell RG, Jørgensen KA. 2002. Catalytic asymmetric 1,3-dipolar cycloaddition reactions of azomethine ylides—a simple approach to optically active highly functionalized proline derivatives. *Angewandte Chemie International Edition* 41:4236–38
28. Żmigrodzka M, Sadowski M, Kras J, Desler E, Demchuk OM, et al. 2022. Polar [3+2] cycloaddition between N-methyl azomethine ylide and trans-3,3,3-trichloro-1-nitroprop-1-ene. *Scientiae Radices* 1:26–35
29. Barama L, Bayoud B, Chafaa F, Khorief Nacereddine A, Djerourou A. 2018. A mechanistic MEDT study of the competitive catalysed [4+2] and [2+2] cycloaddition reactions between 1-methyl-1-phenylallene and methyl acrylate: the role of Lewis acid on the mechanism and selectivity. *Structural Chemistry* 29:1709–21
30. Lamri S, Heddam A, Kara M, Yahia W, Khorief Nacereddine A. 2021. The role of the catalyst on the reactivity and mechanism in the Diels–alder cycloaddition step of the povarov reaction for the synthesis of a biological active quinoline derivative: experimental and theoretical investigations. *Organics* 2:57–71
31. Domingo LR. 2016. Molecular electron density theory: a modern view of reactivity in organic chemistry. *Molecules* 21:1319
32. Ríos-Gutiérrez M, Domingo LR. 2019. Unravelling the mysteries of the [3+2] cycloaddition reactions. *European Journal of Organic Chemistry* 2019:267–82
33. Domingo LR, Emamian SR. 2014. Understanding the mechanisms of [3+2] cycloaddition reactions. The pseudoradical versus the zwitterionic mechanism. *Tetrahedron* 70:1267–73
34. Koumbis AE, Gallos J. 2003. 1,3-dipolar cycloadditions in the synthesis of carbohydrate mimics. Part 2: nitrones and oximes. *Current Organic Chemistry* 7:585–628
35. Feuer H. 2001. *Nitrile oxides, nitrones, and nitronates in organic synthesis: novel strategies in synthesis*. Hoboken, New Jersey: John Wiley & Sons. doi: 10.1002/9780470191552
36. Majumder S, Bhuyan PJ. 2012. Stereoselective synthesis of novel annulated thiopyrano indole derivatives from simple oxindole *via* intramolecular 1,3-dipolar cycloaddition reactions of nitrone and nitrile oxide. *Tetrahedron Letters* 53:762–64
37. Alimohammadi K, Sarrafi Y, Tajbakhsh M, Yeganegi S, Hamzehloueian M. 2011. An experimental and theoretical investigation of the regio- and stereoselectivity of the polar [3+2] cycloaddition of azomethine ylides to nitrostyrenes. *Tetrahedron* 67:1589–97
38. Zeroual A, Ríos-Gutiérrez M, El Idrissi M, El Alaoui El Abdallaoui H, Domingo LR. 2019. An MEDT study of the mechanism and selectivities of the [3+2] cycloaddition reaction of tomentosin with benzonitrile oxide. *International Journal of Quantum Chemistry* 119:e25980
39. Yahia W, Nacereddine AK, Liacha M. 2014. Towards understanding the role of lewis acid on the regioselectivity and mechanism for the acetylation reaction of 2-benzoxazolinone with acetyl chloride: a DFT study. *Progress in Reaction Kinetics and Mechanism* 39:365–74
40. Hehre WJ. 1976. Ab initio molecular orbital theory. *Accounts of Chemical Research* 9:399–406
41. Fukui K. 1981. The path of chemical reactions - the IRC approach. *Accounts of Chemical Research* 14:363–68
42. Reed AE, Curtiss LA, Weinhold F. 1988. Intermolecular interactions from a natural bond orbital, donor-acceptor viewpoint. *Chemical Reviews* 88:899–926
43. Weinhold F. 1998. Natural Bond Orbital Methods. In *Encyclopedia of Computational Chemistry*. Hoboken, New Jersey: John Wiley & Sons. doi: 10.1002/0470845015.cna009
44. Tomasi J, Persico M. 1994. Molecular interactions in solution: an overview of methods based on continuous distributions of the solvent. *Chemical Reviews* 94:2027–94
45. Cancès E, Mennucci B, Tomasi J. 1997. A new integral equation formalism for the polarizable continuum model: Theoretical background and applications to isotropic and anisotropic dielectrics. *The Journal of Chemical Physics* 107:3032–41

46. Frisch MJ, Trucks GW, Schlegel HB, Scuseria GE, Robb MA, et al. 2009. *Gaussian 09, revision A. 02*. Gaussian, Inc, Wallingford
47. Becke AD, Edgecombe KE. 2008. A simple measure of electron localization in atomic and molecular-systems. *Journal of Chemical Physics* 92:5397–403
48. Lu T, Chen F. 2012. Multiwfn: a multifunctional wavefunction analyzer. *Journal of Computational Chemistry* 33:580–92
49. Thomsen DL, Axson JL, Schrøder SD, Lane JR, Vaida V, et al. 2013. Intramolecular interactions in 2-aminoethanol and 3-aminopropanol. *The Journal of Physical Chemistry A* 117:10260–73
50. Contreras-García J, Johnson ER, Keinan S, Chaudret R, Piquemal JP, et al. 2011. NCIPLOT: a program for plotting noncovalent interaction regions. *Journal of Chemical Theory and Computation* 7:625–32
51. Bader RFM, Essén H. 1984. The characterization of atomic interactions. *The Journal of Chemical Physics* 80:1943–60
52. Zawadzińska K, Ríos-Gutiérrez M, Kula K, Woliński P, Mirosław B, et al. 2021. The participation of 3,3,3-trichloro-1-nitroprop-1-ene in the [3+2] cycloaddition reaction with selected nitrile *N*-oxides in the light of the experimental and MEDT quantum chemical study. *Molecules* 26:6774
53. Mirosław B, Babyuk D, Łapczuk-Krygier A, Kącka-Zych A, Demchuk OM, et al. 2018. Regiospecific formation of the nitromethyl-substituted 3-phenyl-4,5-dihydroisoxazole *via* [3+2] cycloaddition. *Monatshefte Für Chemie - Chemical Monthly* 149:1877–84
54. Yahia W, Nacereddine AK, Liacha M, Djerourou A. 2018. A quantum-chemical DFT study of the mechanism and regioselectivity of the 1,3-dipolar cycloaddition reaction of nitrile oxide with electron-rich ethylenes. *International Journal of Quantum Chemistry* 118:e25540
55. Domingo LR, Sáez JA. 2009. Understanding the mechanism of polar Diels–alder reactions. *Organic & Biomolecular Chemistry* 7:3576–83
56. Domingo LR, Aurell MJ, Pérez P. 2014. A DFT analysis of the participation of zwitterionic TACs in polar [3+2] cycloaddition reactions. *Tetrahedron* 70:4519–25
57. Wiberg KB. 1968. Application of the Pople-santry-Segal CNDO method to the cyclopropylcarbinyl and cyclobutyl cation and to bicyclobutane. *Tetrahedron* 24:1083–96
58. Benchouk W, Mekelleche SM, Silvi B, Aurell MJ, Domingo LR. 2011. Understanding the kinetic solvent effects on the 1,3-dipolar cycloaddition of benzonitrile N-oxide: a DFT study. *Journal of Physical Organic Chemistry* 24:611–18
59. Domingo LR, Saéz JA, Zaragozá RJ, Arnó M. 2008. Understanding the participation of quadricyclane as nucleophile in polar [$2\sigma+2\sigma+2\pi$] cycloadditions toward electrophilic $\pi$ molecules. *Journal of Organic Chemistry* 73:8791–99
60. Khorief Nacereddine A, Sobhi C, Djerourou A, Ríos-Gutiérrez M, Domingo LR. 2015. Non-classical CH···O hydrogen-bond determining the regio- and stereoselectivity in the [3+2] cycloaddition reaction of (*Z*)-*C*-phenyl-*N*-methylnitrone with dimethyl 2-benzylidenecyclopropane-1,1-dicarboxylate. A topological electron-density study. *RSC Advances* 5:99299–311
61. Khorief Nacereddine A, Merzoud L, Morell C, Chermette H. 2021. A computational investigation of the selectivity and mechanism of the Lewis acid catalyzed oxa-Diels-Alder cycloaddition of substituted diene with benzaldehyde. *Journal of Computational Chemistry* 42:1296–311
62. Khorief Nacereddine A. 2020. A MEDT computational study of the mechanism, reactivity and selectivity of non-polar [3+2] cycloaddition between quinazoline-3-oxide and methyl 3-methoxyacrylate. *Journal of Molecular Modeling* 26:328
63. Chafaa F, Khorief Nacereddine A, Djerourou A. 2019. Unravelling the mechanism and the origin of the selectivity of the [3 + 2] cycloaddition reaction between electrophilic nitrone and nucleophilic alkene. *Theoretical Chemistry Accounts* 138:123
64. Rozas I, Alkorta I, Elguero J. 2000. Behavior of ylides containing N, O, and C atoms as hydrogen bond acceptors. *Journal of the American Chemical Society* 122:11154–61
65. Grabowski SJ, Andrzej Sokalski W, Dyguda E, Leszczyński J. 2006. Quantitative classification of covalent and noncovalent H-bonds. *The Journal of Physical Chemistry B* 110:6444–46